International Journal of Solids and Structures 81 (2016) 337–349

Contents lists available at ScienceDirect

International Journal of Solids and Structures

journal homepage: www.elsevier.com/locate/ijsolstr

Thermodynamically consistent elasto-plastic microplane formulation for fiber reinforced concrete

Sonia Vrech[a,b,*], Guillermo Etse[a,b,c], Antonio Caggiano[a,c]

[a] National Scientific and Technical Research Council (CONICET), Argentina
[b] CEMNCI, Faculty of Exact Sciences and Engineering, National University of Tucuman, Argentina
[c] LMNI, Faculty of Engineering, University of Buenos Aires, Argentina

ARTICLE INFO

Article history:
Received 22 July 2015
Revised 5 November 2015
Available online 17 December 2015

Keywords:
Microplanes
Plasticity
Failure
Mixture Theory
Steel Fibers Reinforcement

ABSTRACT

In this work a thermodynamically consistent elasto-plastic microplane constitutive theory, aimed at simulating the failure behavior of Steel Fiber Reinforced Concrete (SFRC), is developed. The continuum (smeared crack) formulation, based on the microplane theory, assumes a parabolic maximum strength criterion in terms of normal and shear (micro-)stresses evaluated on each microplane to simulate the failure behavior of concrete. In the high confinement regime, a non-associated plastic flow rule is also defined in terms of microplane stresses. The well-known "Mixture Theory" is considered to account for the presence of fibers in concrete matrix. The interaction between steel fibers and cracked concrete in the form of fiber-to-concrete bond-slip and dowel mechanisms is taken into account. The complete formulation is fully consistent with the thermodynamic laws. After describing the proposed constitutive theory, numerical analyses at constitutive level of SFRC failure behavior are presented and discussed. Thereby, the variations of the fracture energy, post-peak strength and cracking behavior with the fiber contents are evaluated and compared against experimental data. The attention also focuses on the evaluation of the sensitivity of SFRC failure predictions with the proposed constitutive model regarding fiber orientation on one hand, and the bond-slip bridging actions and dowel mechanism on the other hand.

1. Introduction

The development of innovative composites based on further enhancing of cementitious materials represents a new challenging and interesting field of the Material Science and the Structural Engineering. Most significant examples are the High Performance Concretes (HPC) and, particularly, the Steel Fiber Reinforced Concrete (SFRC) (Gettu, 2008; Li et al., 1998a, 1998b; Mirsayah and Banthia, 2002). Actually, the application of SFRC in civil and military constructions have significantly increased in the last decades (and that trend still continues). The well-known deficiencies of cement-based materials like concretes, i.e., low strength and brittle response in low confinement and tensile regimes, can be mitigated by adding short steel fibers randomly distributed into the cementitious mortar. The major advantages of SFRC, as compared with plain concretes, is its higher residual tensile strength accompanied with elevated toughness in post-cracking regime (Naaman and Reinhardt, 2006; Nguyen et al., 2010; di Prisco et al., 2009). Since fiber bridging mechanisms mainly take place under cracked regime of concrete matrix, the mechanical behavior of uncracked members is practically not influenced by the addition of fibers beyond the limited increase of the elastic stiffness.

In the last years, many constitutive theories were proposed for failure analysis of SFRC. Most of them follow the Smeared Crack Approach (SCA) and, particularly, the flow theory of plasticity (Hu et al., 2003; Seow and Swaddiwudhipong, 2005) and the continuum damage theory, see also the work by Li and Li (2001). Besides the SCA-based proposals, several constitutive models and theoretical formulations are based on the Discrete Crack Approach (DCA). In the DCA the kinematic of cracking is modeled by means of the displacement field in discontinuities or interfaces in the finite element discretization, see also the contributions by Prasad and Krishnamoorthy (2002) and Etse et al. (2012).

The failure behavior of SFRC was evaluated not only at the macroscopic level of observation but also at the mesoscopic one. We may here refer to the contributions by Leite et al. (2004) and Schauffert and Cusatis (2012) who considered the effect of fibers dispersed into a Lattice Discrete Particle Model (LDPM), by Oliver et al. (2012) who highlighted the macroscopic response in terms

* Corresponding author at: CEMNCI, Faculty of Exact Sciences and Engineering, National University of Tucuman, Argentina. Tel.: +54 3814245027.
E-mail addresses: svrech@herrera.unt.edu.ar, svrech@hotmail.com (S. Vrech), getse@herrera.unt.edu.ar (G. Etse), acaggiano@fi.uba.ar (A. Caggiano).

http://dx.doi.org/10.1016/j.ijsolstr.2015.12.007
0020-7683/

of the meso-structural phenomenon associated with the fiber–matrix bond-slip action, by Gal and Kryvoruk (2011) who proposed a mesoscale two-step homogenization approach and the proposals by Radtke et al. (2010) and Cunha et al. (2012) whereby the SFRC has been considered as a two-phase material. A discrete crack model to predict failure behavior of SFRC based on "Mixture Theory" concepts allowing both macroscopic and mesoscopic analysis has been proposed by the authors (Caggiano et al., 2012; Etse et al., 2012).

During the last decades, the well-known microplane theory has largely been used for predicting the mechanical behavior of quasi-brittle materials such as concrete or rocks. Pioneer contributions of the microplane theory in constitutive formulations for concrete materials are represented by the works by Bažant and Gambarova (1984), Bažant and Oh (1985), Carol et al. (1992), and more recently by Carol and Bažant (1997), Kuhl and Ramm (2000) and Cervenka et al. (2005). A well-established thermodynamically consistent approach has been described by Carol et al. (2001) and Kuhl et al. (2001). Other relevant microplane-based contributions can be found in several applications including concrete failure prediction under cyclic loads (Ožbolt et al., 2001), numerical analyses of compressed concrete columns confined with carbon fiber reinforced polymers (Gambarelli et al., 2014), the mechanical response of polycrystalline shape memory alloys (Brocca et al., 2002), micropolar continua formulation in the spirit of Cosserat Media (Etse and Nieto, 2004; Etse et al., 2003), strain-softening nonlocal models (Bažant and Di Luzio, 2004; Di Luzio, 2007), large strains (Carol et al., 2004), as well as non-linear hardening–softening behavior of fiber reinforced concretes (Beghini et al., 2007; Caner et al., 2013). Although (Caner et al., 2013) these describe the behavior and fracturing of SFRC under not only uniaxial but also general multiaxial loading, they mainly include the fiber pull-out and breakage effects.

The present work formulates a novel thermodynamically consistent fracture-based microplane model for simulating the failure behavior of SFRC. The constitutive formulation at the microplane level is described in terms of normal and shear stresses vs. related micro-strains. Fiber effect on the composite failure behavior is taken into account through both a bond-slip formulation and a dowel model depending on the relative orientations between fibers and microplanes. The general basis of the proposed microplane theory for SFRC are presented in Section 2. Section 3 is related to the application of the well-known "Mixture Theory" by Truesdell and Toupin (1960) to describe the mechanical behavior of SFRC, following previous contributions by Oliver et al. (2008) and Vrech et al. (2010). Particularly, Section 3.1 reports the constitutive laws employed at microplane level featuring the fracture-based softening formulation for plain concrete, while the model description of the fiber-to-concrete interactions, approximating throughout debonding mechanisms and dowel effects of fibers crossing cracks, are highlighted in Sections 3.2–3.4. All constitutive laws of the different constituents are formulated within the thermodynamic framework. This encompasses both the elastic and inelastic portions of the internal material laws of the proposed constitutive theory. Finally, Section 4 covers the numerical analysis with the proposed constitutive model. The predictive capabilities and soundness of the proposal at constitutive level are addressed and discussed against experimental tests available in scientific literature. Section 4 also includes the numerical sensitive analysis of the model predictions regarding the variation of fiber direction, fiber content, bond-slip and dowel mechanisms.

2. Thermodynamically consistent microplane theory

A thermodynamically consistent elasto-plastic constitutive model based on the microplane theory is proposed for simulating the failure behavior of SFRC. Kinematic assumptions as well as constitutive equations are presented in the following subsections.

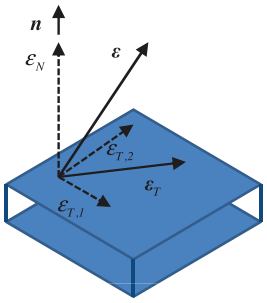

Fig. 1. Strain components at the microplane level.

The microplane approach originally proposed by Bažant and Oh (1983) consists in the formulation of constitutive laws at microplane level defining the mechanical behavior of planes (the microplanes) generically orientated. Then, the macroscopic response shall be achieved through the consideration of appropriated thermodynamically consistent homogenization process over the responses in all microplanes.

2.1. Kinematic assumptions

Assuming kinematic constraints, the normal and tangential strains at microplane level, ε_N and $\boldsymbol{\varepsilon}_T$, respectively, are computed by means of the following relationships:

$$\varepsilon_N = \boldsymbol{N} : \boldsymbol{\varepsilon}^{mac}, \quad \boldsymbol{\varepsilon}_T = \boldsymbol{T} : \boldsymbol{\varepsilon}^{mac} \tag{1}$$

being $\boldsymbol{\varepsilon}^{mac}$ the macroscopic strain tensor projected on a microplane characterized by its normal direction $\boldsymbol{n}$, see Fig. 1.

The projection tensors are defined as

$$\boldsymbol{N} = \boldsymbol{n} \otimes \boldsymbol{n}, \quad \boldsymbol{T} = \boldsymbol{n} \cdot \boldsymbol{I}^{sym} - \boldsymbol{n} \otimes \boldsymbol{n} \otimes \boldsymbol{n} \tag{2}$$

being $\boldsymbol{I}^{sym}$ the symmetric part of the fourth-order identity tensor.

In the elasto-plastic regime and assuming small strains, both macro- and microscopic strains are computed according to the Prandtl–Reuss additive decomposition. Particularly, at microplane level, normal and tangential strain rates are obtained as

$$\dot{\varepsilon}_N = \dot{\varepsilon}_N^e + \dot{\varepsilon}_N^p, \quad \dot{\boldsymbol{\varepsilon}}_T = \dot{\boldsymbol{\varepsilon}}_T^e + \dot{\boldsymbol{\varepsilon}}_T^p \tag{3}$$

where the supra-indexes e and p denote elastic and plastic components, respectively.

2.2. Thermodynamically consistent homogenization

Starting point for the formulation of thermodynamically consistent homogenization, relating the field variables on the microplanes with the macroscopic ones, is the definition of the macroscopic Clausius–Duhem inequality for isothermal processes as

$$\mathscr{D}^{mac} = \boldsymbol{\sigma}^{mac} : \dot{\boldsymbol{\varepsilon}}^{mac} - \dot{\psi}^{mac} \geq 0\,. \tag{4}$$

It sets that the macroscopic dissipation $\mathscr{D}^{mac}$, computed as the subtraction between the stress power, $\boldsymbol{\sigma}^{mac} : \dot{\boldsymbol{\varepsilon}}^{mac}$, and the evolution of the free-energy per unit mass of material $\dot{\psi}^{mac}$, cannot become negative; being $\boldsymbol{\sigma}^{mac}$ the macroscopic stress tensor.

Assuming the macro free-energy potential as the integral of the micro free-energy on a spherical region of unit volume Ω, the micro–macro free-energy relationship, according to Carol et al. (2001), can be expressed as

$$\psi^{mac} = \frac{3}{4\pi} \int_{\Omega} \psi \, \mathrm{d}\Omega \tag{5}$$

being $\psi = \psi(\varepsilon_N^e, \boldsymbol{\varepsilon}_T^e, \boldsymbol{\kappa})$ the free-energy potential at microplane level, expressed in terms of the elastic strain components and the vector of internal variables $\boldsymbol{\kappa}$. The evolution law of the micro free-energy, regarding the kinematic projection of Eq. (1), is given by

$$\dot{\psi} = \left(\boldsymbol{N}\sigma_N + \boldsymbol{T}^T \cdot \boldsymbol{\sigma}_T\right) : \dot{\boldsymbol{\varepsilon}}^{mac} - \mathscr{D} \tag{6}$$

with the constitutive stresses computed as

$$\sigma_N = \frac{\partial \psi}{\partial \varepsilon_N}, \quad \boldsymbol{\sigma}_T = \frac{\partial \psi}{\partial \boldsymbol{\varepsilon}_T} \tag{7}$$

and the microscopic dissipation $\mathscr{D}$, that satisfies the following condition:

$$\mathscr{D} = -\frac{\partial \psi}{\partial \boldsymbol{\kappa}} \cdot \dot{\boldsymbol{\kappa}} \geq 0 \tag{8}$$

being

$$\boldsymbol{\phi} = \frac{\partial \psi}{\partial \boldsymbol{\kappa}} \tag{9}$$

the dissipative micro-stresses.

According to Coleman and Noll (1963) and Coleman and Gurtin (1967), the Clausius–Duhem inequality of Eq. (4) leads to the definition of the macroscopic stress tensor in terms of the microscopic stress components

$$\boldsymbol{\sigma}^{mac} = \frac{\partial \psi^{mac}}{\partial \boldsymbol{\varepsilon}^{mac}} = \frac{3}{4\pi} \int_\Omega \boldsymbol{N}\sigma_N + \boldsymbol{T}^T \cdot \boldsymbol{\sigma}_T \, d\Omega. \tag{10}$$

To avoid the difficulties involved in the analytical solution of Eq. (10), Bažant and Oh (1985) proposed integration techniques, which dealt with the numerical solution of the integral over all possible spatial directions by a weighted sum over a finite number of microplanes

$$\boldsymbol{\sigma}^{mac} \approx \sum_{l=1}^{n_{mp}} \left[\boldsymbol{N}^l \sigma_N^l + \boldsymbol{T}^{T,l} \cdot \boldsymbol{\sigma}_T^l\right] \mathrm{w}^l \tag{11}$$

being n_{mp} the adopted number of microplanes and w^l the corresponding weight coefficients.

2.3. Microplane elasto-plastic constitutive formulation

Assuming a decoupled form of the microscopic free-energy potential corresponding to the elasto-plastic regime, it can be expressed as the sum of both elastic and plastic counterparts

$$\psi = \psi^e(\varepsilon_N^e, \boldsymbol{\varepsilon}_T^e) + \psi^p(\kappa) \tag{12}$$

being κ the scalar internal state variable related to the isotropic hardening/softening behavior.

The elastic contribution is computed as

$$\psi^e = \frac{1}{2} E_N (\varepsilon_N^e)^2 + \frac{1}{2} E_T \, \boldsymbol{\varepsilon}_T^e \cdot \boldsymbol{\varepsilon}_T^e \tag{13}$$

where the elastic normal and tangential micro-modules, E_N and E_T, are defined according to Leukart (2005) as

$$E_N = 3K, \quad E_T = \frac{10}{3G} - 2K \tag{14}$$

being K and G the bulk and shear macroscopic moduli, respectively.

The fully uncoupled normal and tangential stress components at microplane level, conjugated to the corresponding micro-strains are obtained regarding Eqs. (7) and (13) as

$$\sigma_N = E_N \varepsilon_N^e, \quad \boldsymbol{\sigma}_T = E_T \boldsymbol{\varepsilon}_T^e \,. \tag{15}$$

According to the plasticity flow theory, the evolution laws of the plastic strain components and the internal variable, under consideration of a convex yield function Φ and a plastic potential Φ^*, result

$$\dot{\varepsilon}_N^p = \dot{\lambda} \frac{\partial \Phi^*}{\partial \sigma_N}, \quad \dot{\boldsymbol{\varepsilon}}_T^p = \dot{\lambda} \frac{\partial \Phi^*}{\partial \boldsymbol{\sigma}_T}, \quad \dot{\kappa} = \dot{\lambda} \frac{\partial \Phi^*}{\partial \phi} \tag{16}$$

being $\dot{\lambda}$ the non-negative plastic multiplier parameter. Complementary, the classical Kuhn–Tucker loading/unloading and the consistency conditions must be considered

$$\Phi \leq 0, \quad \dot{\lambda} \leq 0, \quad \Phi\dot{\lambda} = 0; \quad \dot{\Phi}\dot{\lambda} = 0 \,. \tag{17}$$

From the Prandtl–Reuss additive decomposition of the total strain tensor into the elastic and plastic components of Eqs. (3) and combining Eqs. (9), (15) and (16) follow the constitutive equations in rate form

$$\dot{\sigma}_N = \dot{\sigma}_N^e - \dot{\lambda} E_N \frac{\partial \Phi^*}{\partial \sigma_N} \,, \tag{18}$$

$$\dot{\boldsymbol{\sigma}}_T = \dot{\boldsymbol{\sigma}}_T^e - \dot{\lambda} E_T \frac{\partial \Phi^*}{\partial \boldsymbol{\sigma}_T} \,, \tag{19}$$

$$\dot{\phi} = \frac{\partial \phi}{\partial \kappa} \dot{\kappa} \,. \tag{20}$$

3. Composite constitutive formulation for SFRC

In this section, the microplane constitutive formulation for SFRC based on the Mixture Theory by Truesdell and Toupin (1960) is presented. Main assumption of this theory is that in every infinitesimal volume the kinematic field of the equivalent continuum and that one of each mixture constituent agree. Thus, the stress vector of the mixture is defined as

$$\boldsymbol{t}_\sigma = \omega^m \boldsymbol{\sigma}^m + \omega^f \left[\sigma_N^f \boldsymbol{n} + \boldsymbol{\sigma}_T^f \cdot \boldsymbol{n}_T\right] \tag{21}$$

being ω^m and ω^f the weighting functions depending on the volume fraction of each constituent, with m and f referring to concrete matrix and fibers, respectively. The concrete matrix stress vector is computed as $\boldsymbol{\sigma}^m = [\sigma_N^m \quad \boldsymbol{\sigma}_T^m]$; then, σ_N^f and $\boldsymbol{\sigma}_T^f$ mean the bond-slip and dowel stresses due to the post-cracking interaction between fibers and mortar. These stress components are defined in the normal and tangential directions of the fibers, respectively, same as the vectors $\boldsymbol{n}$ and $\boldsymbol{n}_T$.

3.1. Fracture energy-based thermodynamic model for plain concrete

This section is aimed at describing the fracture energy-based plasticity formulation for plain concrete which relates the normal and tangential micro-stress components with the corresponding microstrains.

Contrarily to Caner et al. (2013), which establish four different boundaries for normal, tangential, volumetric and deviatoric stresses, a unique function based on the parabolic Drucker-Prager yield criterion is proposed in this work for the maximum strength surface at microplanes, incorporating normal and tangential stresses, as can be observed in Fig. 2.

The mathematical expression of the parabolic failure criterion for plain concrete in terms of the normal and tangential micro-stresses σ_N^m and $\boldsymbol{\sigma}_T^m$, respectively, is

$$\Phi^m = ||\boldsymbol{\sigma}_T^m||^2 + m_0 \, \sigma_N^m - c_0 = 0 \,. \tag{22}$$

The calibration of the frictional and cohesive parameters m_0 and c_0 in terms of the uniaxial tensile strength f_t' and the simple shear strength f_s' leads to

$$m_0 = \frac{f_s'^2}{f_t'} \quad \text{and} \quad c_0 = f_s'^2 \,. \tag{23}$$

In the post-peak regime, the yield criterion softens and it is defined as

$$\Phi^m = ||\boldsymbol{\sigma}_T^m||^2 + m_0 \, \sigma_N^m - \phi^m = 0 \tag{24}$$

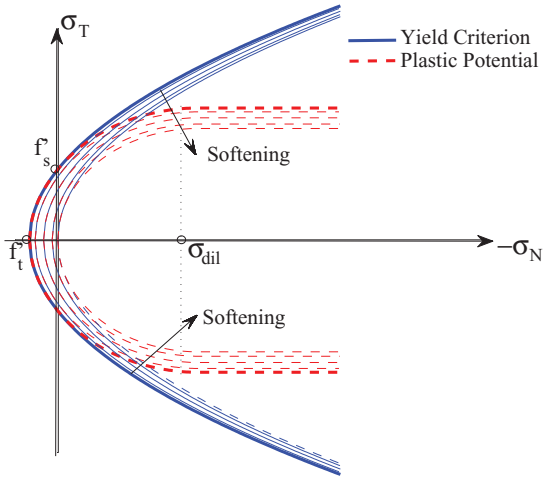

Fig. 2. Yielding criterion, post-cracking and plastic potential evolutions for plain concrete.

being ϕ^m the softening dissipative stress in terms of the internal state variable κ^m. The strength degradation during post-peak processes is controlled by ϕ^m, see Fig. 2.

The plastic flow rule of the model encompasses three different regions in the stress space, as follow:

- tensile regime ($\sigma_N^m \geq 0$): associated rule is considered, i.e. $\Phi^{*m} = \Phi^m$;
- low-confinement regime ($0 > \sigma_N^m \geq \sigma_{dil}$, with σ_{dil} the compressive stress corresponding to the zero concrete dilatancy): volumetric non-associated flow is considered, with

$$\Phi^{*m} = \Phi^m - 2\, m_0 \frac{\sigma_N^{m2}}{\sigma_{dil}} = 0; \tag{25}$$

- medium and high confinement regime ($\sigma_{dil} > \sigma_N^m$): the plastic potential corresponds to the isochoric plastic flow, being

$$\Phi^{*m} = \Phi^m + m_0\left(\frac{\sigma_{dil}}{2} - \sigma_N^m\right) = 0. \tag{26}$$

The plastic component of the Helmholtz free-energy density in Eq. (12) for the concrete component of the mixture is defined as

$$\psi^{m,p} = \frac{c_0}{\alpha_f}\exp\left(-\alpha_f \varepsilon^f\right) \quad \text{with} \quad \alpha_f = 5\frac{h_f}{u_r}, \tag{27}$$

being ε^f the equivalent fracture strain defined as

$$\varepsilon^f = \kappa^m \frac{\partial \Phi^{*m}}{\partial \sigma_N^m}, \tag{28}$$

while u_r represents the maximum crack opening displacement in mode I type of failure and h_f the characteristic length associated to the active fracture process under general mode II type of failure, computed as

$$h_f = \frac{h_t}{R_G} \tag{29}$$

being h_t the characteristic length in mode I type of failure. The fracture energy-based characteristic lengths h_f and h_t represent the distance between active cracks. Thus, under mode I type of failure the maximum value h_t of the characteristic length is obtained. Under mode II or mixed failure mode the dependence of h_f on h_t is defined in terms of the ratio between the fracture energies $R_G = G_f^{II}/G_f^I$. R_G is computed in terms of the acting confining pressure on the microplanes represented by $p^* = \sigma_N^m/f_c'$, being f_c' the uniaxial compressive strength of concrete, see Vrech and Etse (2009), as

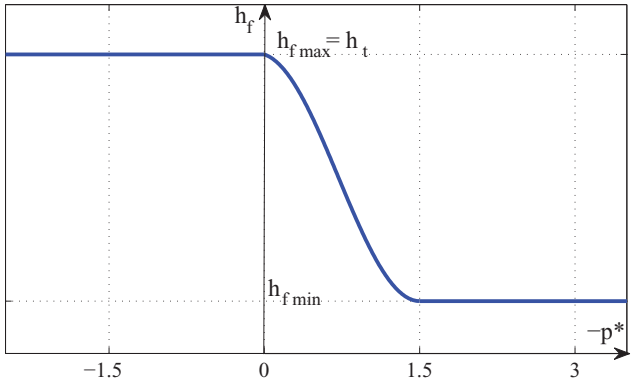

Fig. 3. Variation of h_f with the confinement pressure.

$$R_G(p^*) = \frac{G_f^{II}}{G_f^I} = \begin{cases} 1 & p^* \geq 0\,, \\ 59.74 + 49.74\,\sin\left(2p^* - \frac{\pi}{2}\right) & -1.5 \leq p^* < 0\,, \\ 100 & p^* < -1.5\,. \end{cases} \tag{30}$$

Summarizing:

- Mode I type of failure $\rightarrow h_f = h_t$;
- Mode II type of failure $\rightarrow h_f = h_t/R_G$.

The variation of h_f with increasing confining pressure is shown in Fig. 3.

The dissipative stress obtained combining Eqs. (9) and (27) results

$$\phi^m = c_0 \exp\left(\alpha_f \kappa^m\right). \tag{31}$$

3.2. Thermodynamically consistent crack-bridging effects of fibers crossing cracks

Steel fibers crossing active opened cracks, bring relevant bridging effects on the overall SFRC post-peak toughness. In this work, the bond-slip mechanism between fibers and concrete matrix is taken into account by means of the axial (tensile) fiber stress σ_N^f. Besides, the dowel effect is considered as a shear transfer mechanism within active cracks. Simple one-dimensional, thermodynamically consistent elasto-plastic constitutive models are proposed in the followings subsections for both interaction mechanisms.

3.3. One-dimensional thermodynamic bond-slip model

The proposed elasto-plastic bond-slip constitutive model is defined by means of the following equations:

$$\psi_N^f = \frac{1}{2}E^f\left(\varepsilon_N^{f,e}\right)^2 + \frac{1}{2}H_N^f\left(\kappa_N^f\right)^2 \quad \text{(free-energy potential)} \tag{32}$$

$$\sigma_N^f = E^f\left(\varepsilon_N^{f,e} - \varepsilon_N^{f,p}\right) \quad \text{(constitutive relation)} \tag{33}$$

$$\Phi_N^f = |\sigma_N^f| - \left(\sigma_y^f + \phi_N^f\right) \leq 0 \quad \text{(yield function)} \tag{34}$$

$$\dot{\kappa}_N^f = \dot{\lambda} \quad \text{(internal variable evolution)} \tag{35}$$

$$\dot{\phi}_N^f = H_N^f \dot{\kappa}^f \quad \text{(softening law)} \tag{36}$$

where $\varepsilon_N^{f,e}$ and $\varepsilon_N^{f,p}$ are the elastic and plastic axial strains, respectively, E^f the elastic module, σ_y^f the equivalent yield stress and H_N^f the hardening/softening parameter; whereas κ_N^f is the internal variable, conjugated to the dissipative stress ϕ_N^f.

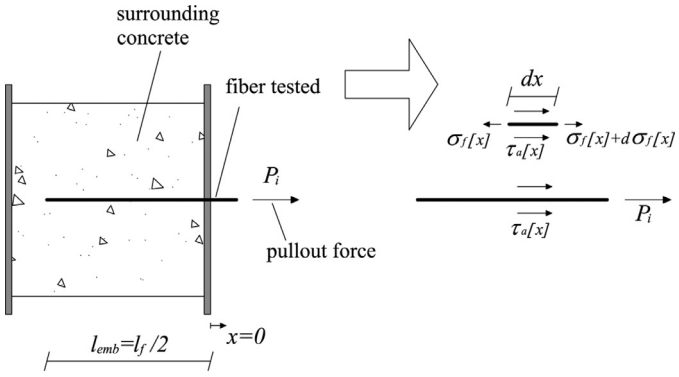

Fig. 4. Pull-out of a single fiber.

According to Oliver et al. (2008), slipping-fibers and fiber–concrete interfaces define a serial system, whereby the fiber total strain ε_N^f is assumed as the sum of the proper fiber deformation ε^d and the interface sliding ε^i, $\varepsilon_N^f = \varepsilon^d + \varepsilon^i$. Whereas the fiber stress σ_N^f is identical on each component $\sigma_N^f = \sigma_N^d = \sigma_N^i$. The material mechanical features of this serial system defining the considered bond-slip model result

$$E^f = \frac{1}{1/E^d + 1/E^i} \tag{37}$$

$$\sigma_y^f = \min[\sigma_y^d; \sigma_y^i] \tag{38}$$

$$H_N^f = \begin{cases} H_N^d, & \text{if } \sigma_y^d < \sigma_y^i \\ H_N^i, & \text{otherwise} \end{cases} \tag{39}$$

where the superscripts d and i denote fiber and interface, respectively.

3.3.1. Pull-out analysis of a single fiber

Pull-out analysis of a single fiber is reported in this subsection. Particularly, Fig. 4 deals with an isolated fiber loaded by an axial force, P_i. The fiber is embedded in a cementitious matrix for a l_{emb} length measure. Thus, the equilibrium scheme proposed in Fig. 4, is used to simulate the complete slipping behavior.

The following basic equations are used for analyzing the overall fiber-to-concrete debonding process:

- *Equilibrium*: $\frac{d\sigma_f[x]}{dx} = -\frac{4\tau_a[x]}{d_f}$, being σ_f the axial stress of the fiber at a certain value of the abscissa x, τ_a the shear bond stress and d_f the diameter of the fiber.
- *Fiber constitutive law in the axial direction*: $\sigma_f[x] = E^d \frac{ds[x]}{dx}$, with E^d the elastic steel modulus and $s[x]$ the slip between fiber and surrounding concrete mortar based on the assumption of Fig. 4.
- *Bi-linear bond constitutive law*: $\tau_a[x] = \begin{cases} -k_E\, s[x] & s[x] \le s_e \\ -\tau_{y,a} + k_S(s[x] - s_e) & s_e < s[x] \le s_u, \\ 0 & s[x] > s_u \end{cases}$ where k_E and $-k_S$ represent the slope of the elastic and softening branches of the bond-slip relationship, respectively, and $\tau_{y,a}$ is the maximum shear stress. Thus, $s_e = \frac{\tau_{y,a}}{k_E}$ and s_u represent the elastic and the ultimate slips, respectively.

As schematically reported in Table 1 and based on the approach proposed by Caggiano and Martinelli (2012), different states of the bond response can be defined. Particularly, the fiber-to-concrete interface is in elastic bond state (E) if $s[x] \le s_e$, in softening state (S) when $s_e < s[x] \le s_u$ or the bond is crushed if $s[x] > s_u$. A combination of these three stress states can actually occur throughout the bonding length during the pull-out process of the single fiber (see Table 1).

Table 1
Bond response of the fiber–concrete joint depending on the slip $s[x]$ developed throughout the embedment length.

Slips	Type of joint adherence
$s[x] \le s_e \,\forall x \in [-l_{emb}, 0]$	Elastic response (E)
$s[x] \le s_e \,\forall x \in [-l_{emb}, -l_e]$	
$s_e < s[x] \le s_u \,\forall x \in [-l_e, 0]$	Elastic–softening response (ES)
$s_e < s[x] \le s_u \,\forall x \in [-l_{emb}, 0]$	Softening response (S)
$s[x] \le s_e \,\forall x \in [-l_{emb}, -l_e]$	
$s_e < s[x] \le s_u \,\forall x \in [-l_e, -l_u]$	Elastic–softening–debonding (ESD)
$s[x] > s_u \,\forall x \in [-l_u, 0]$	
$s_e < s[x] \le s_u \,\forall x \in [-l_{emb}, -l_u]$	
$s[x] > s_u \,\forall x \in [-l_u, 0]$	Softening–debonding response (SD)
$s[x] > s_u \,\forall x \in [-l_{emb}, 0]$	Debonding failure (D)

Being $-l_e (0 \le l_e \le l_{emb})$ and $-l_u (0 \le l_u \le l_{emb})$ the abscissas of the points in which the local slip $s[x]$ is equal to the elastic limit (s_e) and the ultimate value (s_u), respectively.

Fully elastic behavior of fibers is assumed. This is strictly true in the case of synthetic fibers, while can be accepted for steel ones when the length l_{emb} results in the condition that $P_{i,max} \le \sigma_y^d A_f$, being σ_y^d the yielding stress and A_f the area of the fiber cross section.

The proposed unified formulation has been intended as a key element to be employed in the 1D model proposed in Section 3.3 to explicitly simulate the mechanical behavior of FRC by taking into account the discrete nature of such materials and the contributions of the various constituents within the framework of the so-called meso-mechanical approach.

In particular, the equivalent yield stress σ_y^f, the hardening/softening parameter H_N^f and E^f of Eqs. (37)–(39) follow from the bond-slip model outlined in this subsection. For the sake of simplicity, the description of the complete analytical pull-out model is omitted in this work but may be obtained from Caggiano and Martinelli (2012). Thereby the complete bond model representing the interaction between fibers and surrounding mortar under pull-out action is described. On the other hand, the link between Section 3.3 and 3.3.1 have been outlined in Caggiano (2013).

3.4. Constitutive model for fiber dowel effect

The following one-dimensional elasto-plastic formulation is considered to take into account the dowel effect of fibers crossing open cracks in cementitious matrix.

The thermodynamically consistent constitutive model proposed in this work is based on the following equations

$$\psi_T^f = \frac{1}{2} G^f \boldsymbol{\varepsilon}_T^{f,e} \cdot \boldsymbol{\varepsilon}_T^{f,e} + \frac{1}{2} H_T^f \left(\kappa_T^f\right)^2 \quad \text{(free-energy potential)} \tag{40}$$

$$\boldsymbol{\sigma}_T^f = G^f (\boldsymbol{\varepsilon}_T^{f,e} - \boldsymbol{\varepsilon}_T^{f,p}) \quad \text{(constitutive relation)} \tag{41}$$

$$\Phi_T^f = |\, \boldsymbol{\sigma}_T^f \,| - (\tau_y^f + \phi_T^f) \le 0 \quad \text{(yield function)} \tag{42}$$

$$\dot{\kappa}_T^f = \dot{\lambda} \quad \text{(internal variable evolution)} \tag{43}$$

$$\dot{\phi}_T^f = H_T^f \dot{\kappa}_T^f \quad \text{(softening law)} \tag{44}$$

being $\boldsymbol{\varepsilon}_T^{f,e}$ and $\boldsymbol{\varepsilon}_T^{f,p}$ the elastic and plastic shear strain, respectively, κ_T^f the internal variable conjugated to the dissipative stress ϕ_T^f and H_T^f, once again, the hardening/softening parameter. The adopted dowel stiffness G_f and the equivalent strength τ_y^f characterizing the dowel mechanism, are based on the definition of both stiffness and strength of a generic fiber embedded in a concrete matrix and subjected to a transverse force. This formulation is developed in analogy to a "semi-infinite" beam on a Winkler foundation following the empirical work by El-Ariss (2007) and the experimental

contributions by Dei Poli et al. (1992), Soroushian et al. (1987) and Dulacska (1972).

3.4.1. Dowel stiffness

To have a more understanding of the dowel stiffness G^f, the following differential equation for the deflection equilibrium of a Winkler's beam can be written as

$$\frac{d^4\Delta(x)}{x^4} + 4\lambda_\omega^4\Delta(x) = 0 \qquad \text{with} \qquad \lambda_\omega^4 = \frac{k_c}{4E^d J_s} \tag{45}$$

being $\Delta(x)$ the deflection of the beam, k_c the elastic stiffness of the spring foundation modeling the surrounding cementitious matrix, E^d and J_s are the elastic modulus of the steel and the inertia of the fiber, respectively, and finally λ_ω represents a characteristic length of the Winkler beam.

The fiber is analyzed as a "semi-infinite" beam on Winkler foundation, then the following equations govern the problem

$$\begin{aligned}\Delta(x) &= A_1\, e^{-\lambda_\omega x}\cos(\lambda_\omega x) + A_2\, e^{-\lambda_\omega x}\sin(\lambda_\omega x)\\ M_d(x) &= 2\,E^d J_s\,\lambda_\omega^2\, e^{-\lambda_\omega x}[A_2\cos(\lambda_\omega x) - A_1\sin(\lambda_\omega x)]\\ V_d(x) &= -2\,E^d J_s\,\lambda_\omega^3\, e^{-\lambda_\omega x}[(A_2 - A_1)\sin(\lambda_\omega x)\\ &\quad + (A_1 + A_2)\cos(\lambda_\omega x)]\end{aligned} \tag{46}$$

being M_d and V_d the bending moment and the dowel action at $l_f/2$ of the steel fiber, while A_1 and A_2 are constants deriving by the boundary conditions.

The analytical solution of the semi-infinite Winkler's beam problem is based on the assumption that the crack width is considered null and supposing that in $x = 0$ the moment is null (inflection point). Then, considering an applied dowel force, V_d, at the loaded-end $(x = 0)$, the following analytical displacement field is obtained

$$\Delta(x) = -\frac{e^{-\lambda_\omega x}\cos(\lambda_\omega x)}{2\,\lambda_\omega^3\,E^d J_s}\,V_d. \tag{47}$$

Finally, the $V_d - \Delta$ law in correspondence of the considered crack $(x = 0)$ takes the following analytical form

$$V_d = \lambda_\omega^3\,E^d J_s\,\Delta \rightarrow \frac{V_d}{A_f} = \frac{l_f}{A_f}\lambda_\omega^3\,E^d J_s\,\frac{\Delta}{l_f} \Rightarrow G^f = \frac{l_f}{A_f}\,\lambda_\omega^3\,E^d J_s \tag{48}$$

also expressed in terms of $\sigma_T^f - \varepsilon_T^f$ $(\frac{V_d}{A_f} - \frac{\Delta}{l_f})$ law, from which the dowel stiffness, G^f, can be derived. In Eq. (48) $A_f = \pi\,\frac{d_f^2}{4}$ is the cross sectional area of a single fiber.

Moreover, the elastic foundation stiffness of the surrounding concrete, k_c, may be obtained from the empirical expression given in Soroushian et al. (1987) as

$$k_c = \kappa_1\frac{\sqrt{f_c'}}{{d_f}^{2/3}} \tag{49}$$

being f_c' the compression strength of the surrounding cementitious composite and κ_1 a coefficient to be calibrated.

3.4.2. Dowel strength

Finally, the equivalent dowel strength τ_y^f can be defined from the dowel action as

$$\tau_y^f = \frac{V_{d,u}}{A_f} \tag{50}$$

being $V_{d,u}$ the dowel force capacity which is obtained as proposed from the following expression:

$$V_{d,u} = k_{dow}\,d_f^2\sqrt{|f_c'||\sigma_y^d|} \tag{51}$$

being k_{dow} a non-dimensional coefficient which according to (Dulacska, 1972), for the case of RC components, is well described by the value $k_{dow} = 1.27$.

It should be noted that Eq. (51) describes the failure mechanism of the fiber dowel by means of two effects: the local crushing of the surrounding matrix and the yielding of the steel fiber.

4. Numerical analysis

This section illustrates the main features and capabilities of the proposed formulation comparing some numerical results against experimental data available in the literature. For the purpose of these numerical analyses the algorithmic tangent operator of the proposed thermodynamically consistent microplane model was implemented at macroscopic levels. The departure point is the formulation of the continuum elasto-plastic tangent operator for microplane constitutive theories by Kuhl et al. (2001), which was extended in this work for the numerical implementation of the proposed model in the framework of the Mixture Theory. In Fig. 5 the flowchart of the numerical implementation of the proposed microplane model is summarized.

Four types of tests were selected to evaluate the predictive capabilities of the proposed model for SFRC failure behavior: uniaxial tensile, simple shear, uniaxial compression and triaxial compression tests. They activate both mode I and mode II type of fracture and, therefore, are very appropriate to analyze the soundness of the proposed mixture constitutive theory. Fig. 6 shows the considered boundary conditions of the four different tests pursued in this work. The considered tests involve prismatic or cylindrical samples (specific dimensions are provided in the description of each test) under plane stress or cylindrical stress conditions, respectively. The two-dimensional formulation by Park and Kim (2003) instead of the spherical one was considered for the microplane distribution, see Fig. 7.

4.1. Tensile test: verification with experimental data

First, numerical analyses of the uniaxial tensile test were carried out on both plain concrete and SFRC. Two different types of steel fibers were considered namely Dramix I and II whose fundamental properties are given in Table 2. The regarded experimental campaign by Li et al. (1998b) and Li and Li (2001) have been performed on prismatic specimens with the dimensions 500 × 100 × 20 mm^3. The model parameters were adjusted according to the experimental data given by the authors, highlighted in the second column of Table 3.

The comparison between model predictions and the experimental data by Li et al. (1998b) and Li and Li (2001) for the uniaxial tensile test in terms of stress–strain diagrams are reported in Fig. 8. The stress–strain responses of SFRC with uniformly distributed Dramix type II steel fibers and fiber contents (ρ_f) of 3.0%, 3.5% and 4.0% are shown on the left hand side of Fig. 8, while the graphics on the right hand side show the model predictions for panels with Dramix type I fibers and fiber contents of 6.0%, 7.0% and 8.0%.

The numerical predictions demonstrate very good agreement with the experimental results. The proposed constitutive model is able to reproduce the increment of toughness and strength in the uniaxial tensile test with increasing fiber content.

It is worth noting that all the numerical curves in these analyses were obtained by only changing the fiber content and/or the fiber type according to the properties given by Li et al. (1998b) and Li and Li (2001).

4.2. Tensile test: fiber orientation sensitivity

In this section the sensitivity of the proposed thermodynamically consistent microplane theory regarding the orientation of fibers in concrete is evaluated. To this end, four different types of

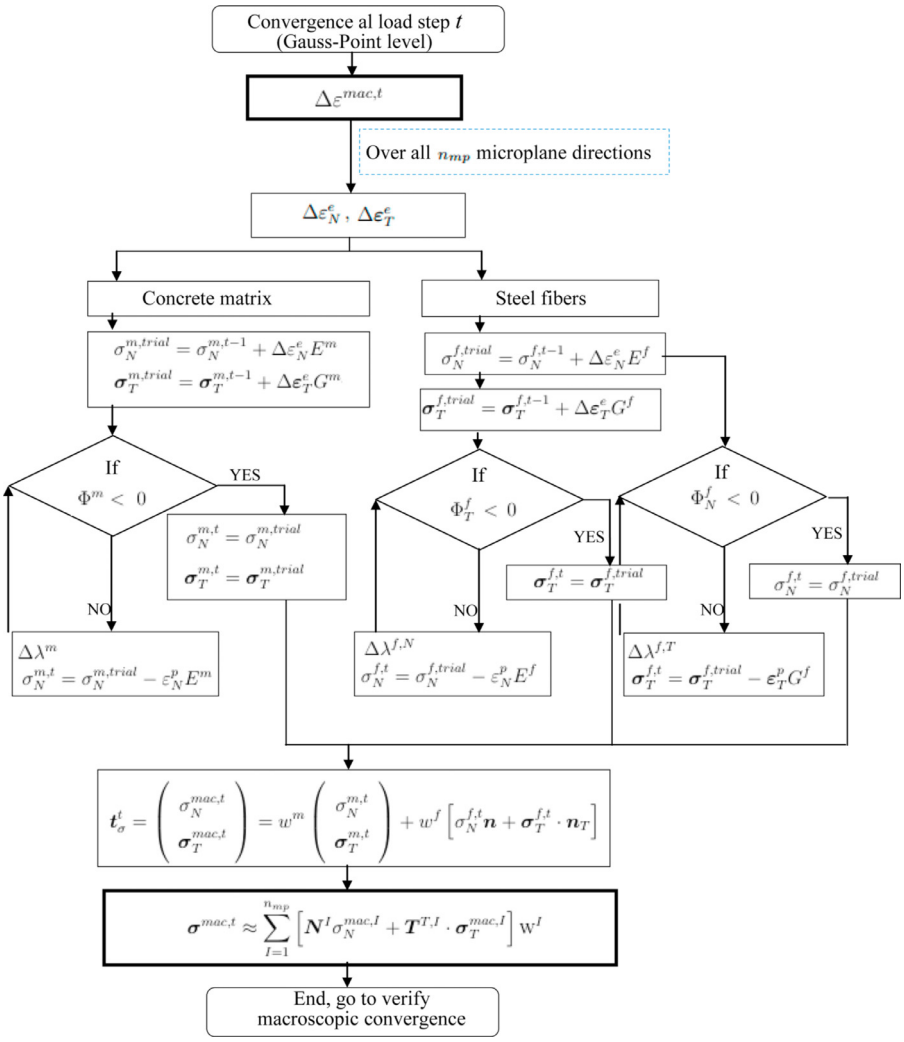

Fig. 5. Flowchart of local Newton's method used for step-by-step integration of the microplane model.

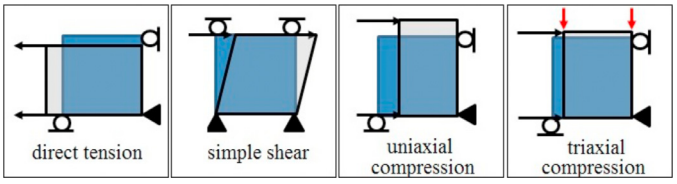

Fig. 6. Load configurations and restraint conditions for uniaxial tension, simple shear, uniaxial and triaxial compression tests.

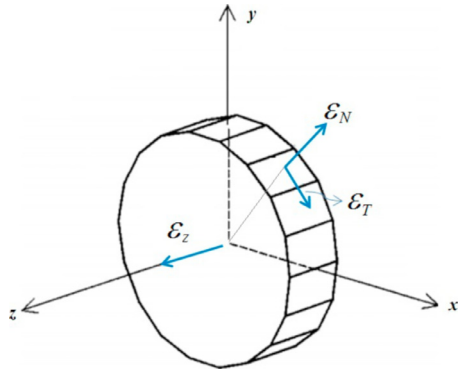

Fig. 7. Two-dimensional microplane model proposed by Park and Kim (2003).

fiber distributions were considered in the uniaxial tensile test, as shown in Fig. 9: uniform or homogeneous distribution of fibers, elliptical distribution of fibers, fibers concentrated in one direction (one microplane at 25°), and fibers located in certain directions (microplanes). In all four cases a total of 42 microplanes were considered while the fiber content was $\rho_f = 7.0\%$.

The results in Fig. 10 show that the mechanical response corresponding to the elliptical distribution of fibers is the one that best matches the uniaxial tensile experimental results by Li et al. (1998b) and Li and Li (2001) performed on SFRC samples. The second most accurate prediction is obtained with the uniform distribution of fibers.

4.3. Tensile test: softening behavior

The *tensile stress–crack width* relationship for SFRC with uniformly distributed fibers ($\rho_f = 2.4\%$) by Abrishambaf et al. (2015) and the corresponding numerical predictions are shown in Fig. 11. This figure depicts the envelope and average curves from the uniaxial tensile test, performed on prismatic probes with dimensions

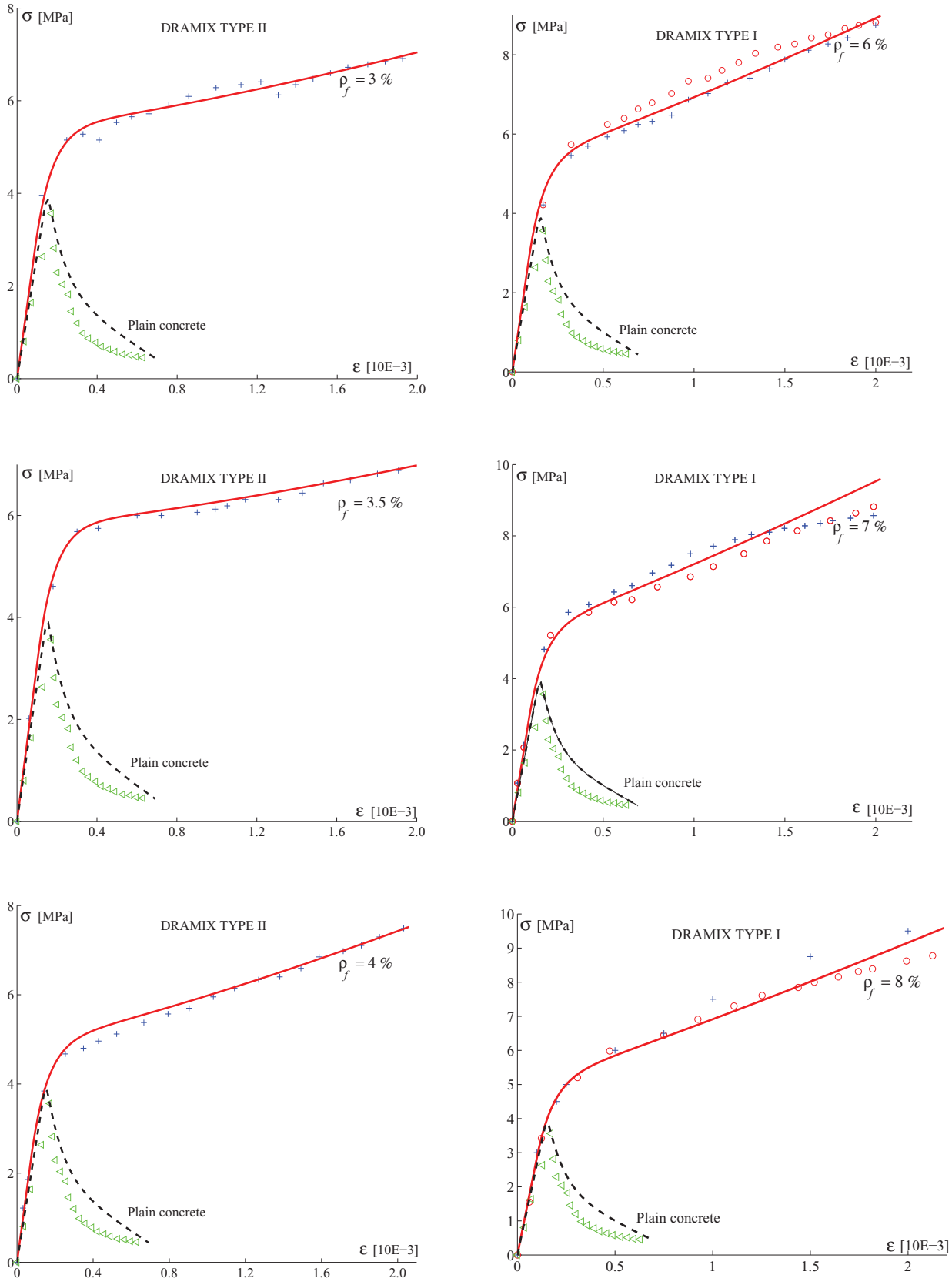

Fig. 8. Tensile tests: verification with experimental data by Li et al. (1998b) and Li and Li (2001) (dotted curves).

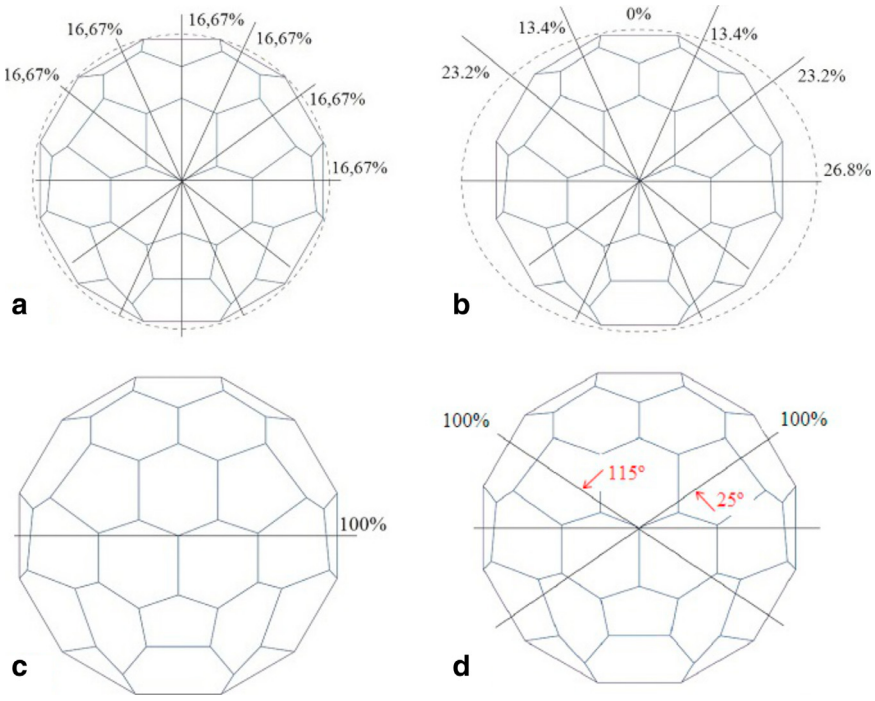

Fig. 9. Types of fiber directional distributions in the uniaxial tensile test: (a) uniform distribution; (b) elliptical distribution; (c) fibers concentrated in one microplane; (d) fibers concentrated in certain microplanes.

Table 2
Characterization of Dramix fibers.

	Density [g/cm^3]	Diameter [mm]	Length [mm]	σ_y^d[GPa]	E^d[GPa]
Dramix type I	7.8	0.5	30	1.20	200
Dramix type II	7.8	0.5	50	1.20	200

Table 3
Characterization of material properties.

Tests	Tensile (Li et al., 1998b)	Tensile (Abrishambaf et al., 2015)	Shear (Mirsayah and Banthia, 2002)	Shear (Soltanzadeh et al., 2015)	Compression (Chern et al., 1992)
Concrete properties					
Elasticity modulus – E^m [GPa]	39.5	34.15	25.0	36.0	20.0
Poisson modulus – ν	0.2	0.2	0.2	0.2	0.2
Compressive strengh – f_c' [MPa]	35.0	47.7	47.0	67.84	20.65
Zero dilatancy stress – σ_{dil} [MPa]	−7.0	−9.0	−9.0	−13.0	−5.0
Tensile rupture displacement – u_r [mm]	0.151	0.160	0.167	0.177	0.130
Crack spacing – h_t [mm]	100	102	150	150	54
Steel fibers properties					
Elasticity modulus – E^d [GPa]	200.0	200.0	200.0	200.0	200.0
Yield stress – σ_y^d [MPa]	1200.0	1100.0	828.0	1100.0	1100.0
Equivalent shear elastic modulus – G^f [GPa]	15.0	15.0	20.6	15.0	15.0
Equivalent shear strength – τ_y^f [MPa]	332.0	441.67	321.0	441.67	330.0
Hardening/softening moduli – $H_N^f = H_T^f$	0.0	0.0	0.0	0.0	0.0
Fiber–concrete interfaces properties					
Elasticity modulus – E^i [GPa]	200.0	200.0	200.0	200.0	200.0
Yield stress – σ_y^i [MPa]	216.0	198.0	149.0	198.0	180.0

110 × 102 × 60 mm^3, as well as the numerical prediction of the proposed microplane-based constitutive theory. The model parameters, based on the material data given by the authors, are summarized in the third column of Table 3.

As can be observed in Fig. 11 the comparison with the experimental results shows very good agreement regarding peak and residual strengths, as well as pre- and post-peak behaviors. The post-cracking stage of SFRC specimens by Abrishambaf et al. (2015) are characterized by a crack-softening behavior which, as a matter of fact, is well captured through the proposed microplane-based model.

4.4. Simple shear test: contribution of the dowel mechanism

The capabilities and efficiency of the proposed microplane model to capture the failure of SFRC is now analyzed by means of the simple shear test. Numerical predictions are shown in terms of shear loads vs. lateral displacements. A total of 42 microplanes with random distribution of fibers have been considered. The adopted material properties correspond to the experimental campaign by Mirsayah and Banthia (2002), performed on 150 × 150 × 500 mm^3 beams. They are displayed in the fourth column of Table 3.

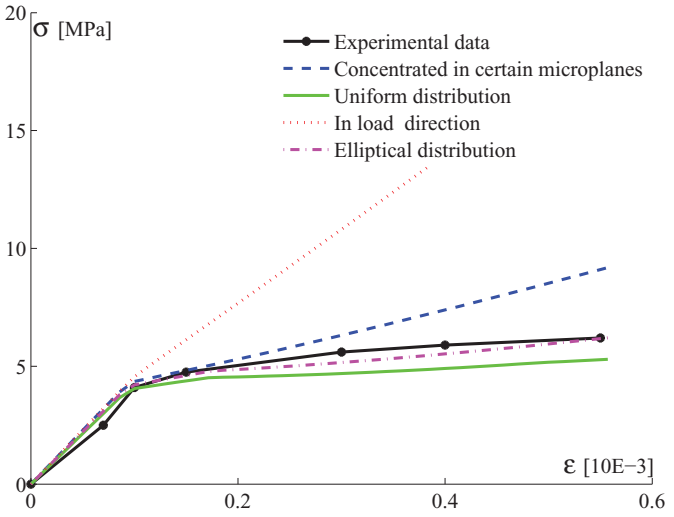

Fig. 10. Prediction of tensile stresses vs. strains of uniaxial tensile test by Li et al. (1998b) and Li and Li (2001) with different types of fiber directional distributions. Dramix type I fibers, $\rho_f = 7.0\%$.

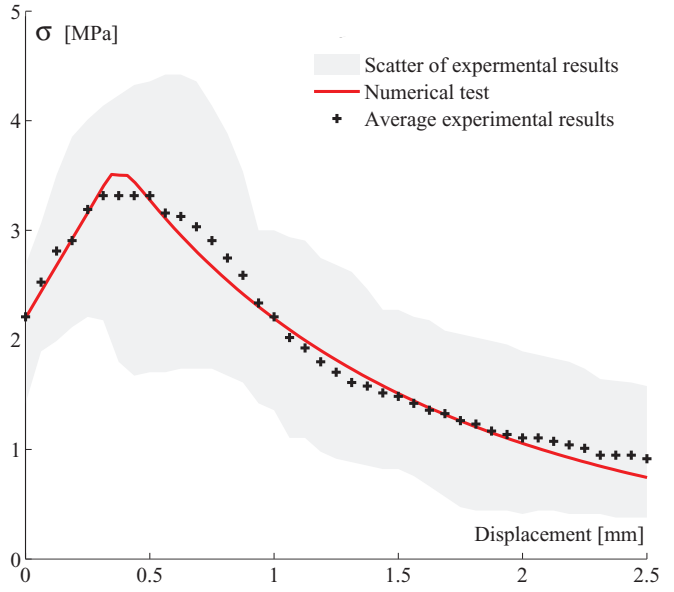

Fig. 11. Prediction of tensile stresses vs. crack opening displacement of uniaxial tensile test by Abrishambaf et al. (2015). Fibers content $\rho_f = 2.4\%$.

Fig. 12 highlights the phenomenological effects of fibers when added in cementitious matrix. The improvement of the composite mechanical behavior in terms of thoughness and also (but slightly) peak strength can be captured by the proposed smeared crack based constitutive theory. Two different fiber contents, i.e. $\rho_f =$ 1.0% and 2.0%, have been considered. The results in Fig. 12 demonstrate the efficiency of the combined microplane-mixture theories to predict the failure behavior of SFRC.

Finally, the contribution of the dowel mechanism of fibers crossing cracks on the overall response behavior is evaluated. To this aim, the numerical simulation of the experimental shear test by Soltanzadeh et al. (2015) is carried out considering the material properties of the fourth column of Table 3.

Fig. 13 compares experimental data (dotted curves) and shear load vs. lateral displacement curves obtained with the microplane-mixture constitutive theory. Two cases are considered. On the one hand, the fiber–mortar interaction is taken into account by means of both fiber-to-concrete bond-slip and dowel mechanisms (blue

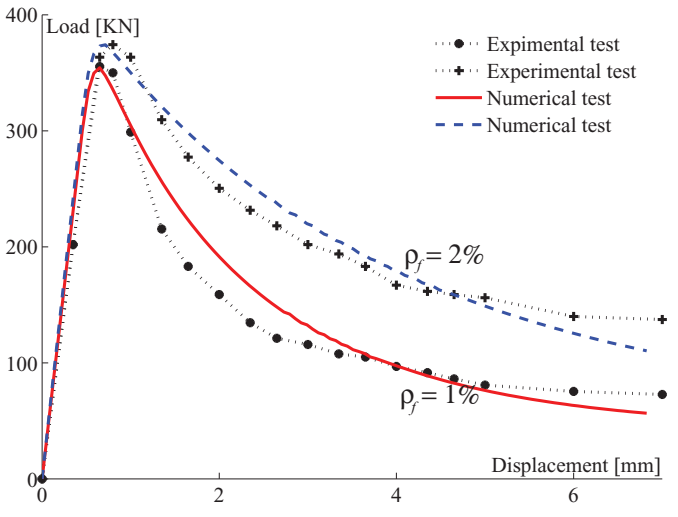

Fig. 12. Shear loads vs. lateral displacements predictions. Comparison with experimental results by Mirsayah and Banthia (2002).

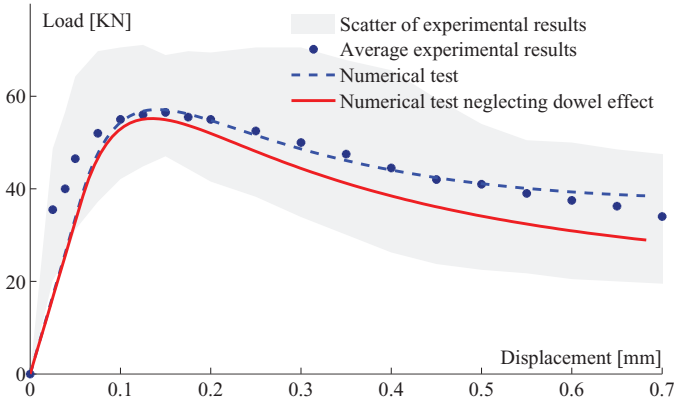

Fig. 13. Contribution of the dowel mechanism in the shear test. Shear load vs. lateral displacement comparison with experimental results by Soltanzadeh et al. (2015), $\rho_f = 4\%$. (For interpretation of the references to color in this figure legend, the reader is referred to the web version of this article.)

dashed curve). On the one hand, the fiber–mortar interaction is modeled only by beans of the bond-slip mechanism while the contribution of the dowel mechanism is neglected (red continuous curve). As can be observed in Fig. 13, when only bond-slip interaction mechanism is taken into account both the shear strength and the thoughness in post-peak decrease, demonstrating the relevant role of the dowel mechanism in the failure behavior of SFRC components under dominant shear.

4.5. Uniaxial and triaxial compression tests

In this section, the predictive capabilities of the proposed material model to reproduce the failure behavior of SFRC are verified, regarding uniaxial and triaxial compression tests. Variable content of steel fibers are considered in the analyses.

Firstly, the numerical predictions of the uniaxial experimental tests by Chern et al. (1992) performed on cylindrical specimens of 58 mm in diameter and 108 mm in height are considered. Corresponding material properties are shown in last column of Table 3. The numerical analysis were performed under cylindrical stress conditions.

Fig. 14 shows the prediction of the proposed model to the uniaxial compression tests for plain concrete and SFRC with 1.0% and 2.0% fiber content. The comparison with the experimental results

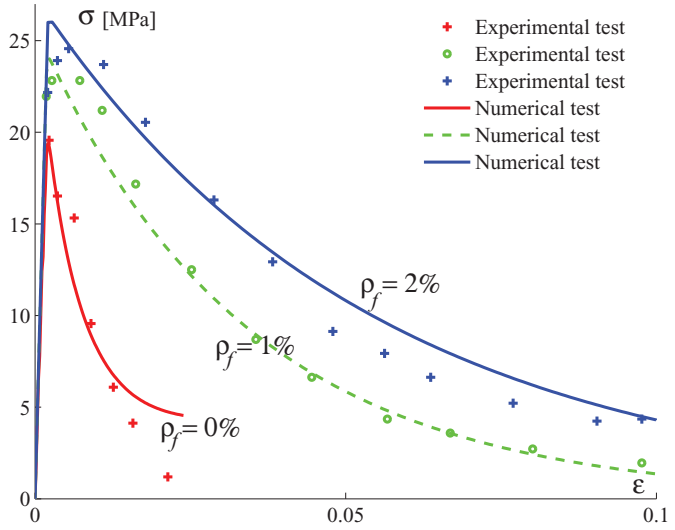

Fig. 14. Predictions of compressive stresses vs. strains of uniaxial compression tests by Chern et al. (1992).

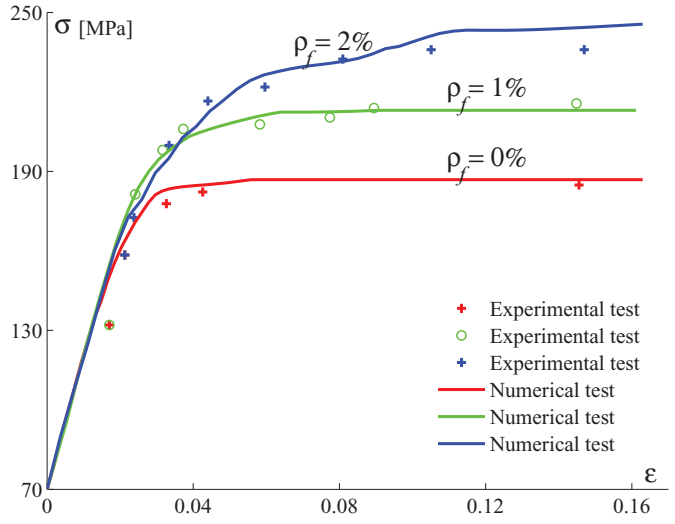

Fig. 15. Prediction of nominal axial stresses vs. axial and radial strains behavior of the triaxial compression tests by Chern et al. (1992).

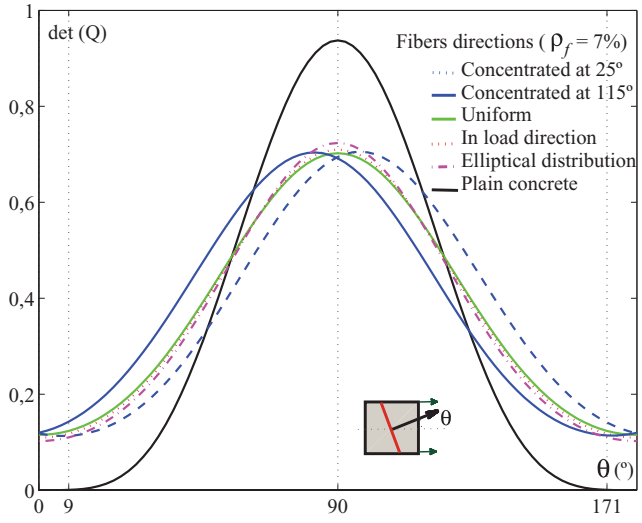

Fig. 16. Numerical localization analysis at peak of the uniaxial tensile test.

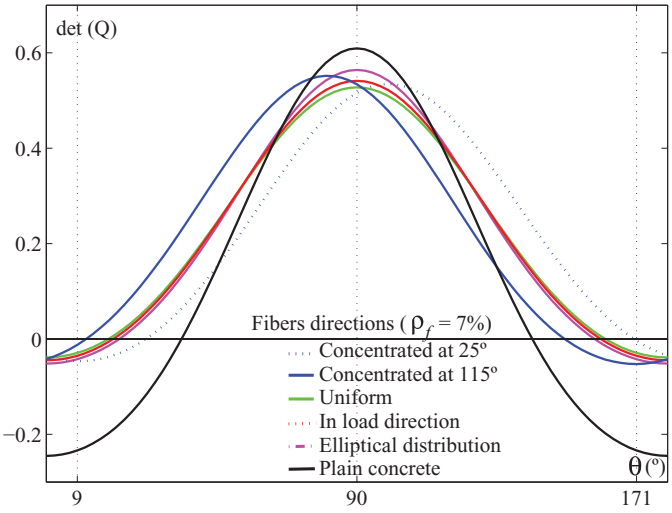

Fig. 17. Numerical localization analysis at residual stress state of the uniaxial tensile test.

shows very good agreement for both, plain concrete and SFRC, regarding peak strength, post-peak behavior and residual strength. From Fig. 14 it can be concluded that the addition of steel fibers to concrete considerably increases the toughness whereas slightly increases the compressive strength and the strain at peak stress.

At this stage it should be noted, according to Nataraja et al. (1999), Neves and de Almeida (2005) and Lee et al. (2015), that the fiber influence on the maximum compressive strength is variable, depending on matrix and fiber characteristics. Strain at peak stress increases with concrete compressive strength, while toughness of higher strength concrete is more sensitive to fiber reinforcement.

Finally, the triaxial compression experimental results by Chern et al. (1992) on concrete cylinders of 100 × 200 mm^2 are considered (Fig. 15). These tests were performed with variable content of fibers, i.e. ρ_f = 0.0%, 1.0% and 2.0% and a lateral confinement of 70 MPa.

It is worth mentioning that while plain concrete and SFRC show a pronounced decrease in stress after peak strength, SFRC exhibits ductile behavior in cases of triaxial compression.

4.6. Discontinuous bifurcation condition

The critical condition for localized failure in the form of discontinuous bifurcation, as highlighted in the Appendix A, is analyzed for plain concrete and SFRC by means of numerical analysis with the proposed model. Main purpose of this analysis is, on one hand, to evaluate the effect of steel fibers on the performance of the localization indicator or on the potential for localized failure. On the other hand, this analysis allows to evaluate the sensitivity of the fiber orientation on the critical condition for discontinuous bifurcation.

Figs. 16 and 17 show the performance of the determinant of the macroscopic normalized localization indicator $\det(\mathbf{Q}) = \det(\mathbf{Q}^{ep})/\det(\mathbf{Q}^{e})$ at peak and residual stress states of the uniaxial tensile test by Abrishambaf et al. (2015). The four different distributions of fiber orientations as shown in Fig. 9 are evaluated regarding their localization indicator performances. The results demonstrate that the proposed microplane-mixture constitutive theory is able to capture the effect of the fiber orientation on the elastic properties degradation, not only regarding the amount of the degradation but also its orientation. This is a relevant characteristic of the proposed material theory.

5. Conclusions

A thermodynamically consistent elasto-plastic microplane constitutive theory aimed at predicting the failure behavior of Steel Fiber Reinforced Concrete (SFRC) has been developed. The model formulation, founded on a macroscopic smeared crack approach and, particularly, on the full thermodynamic consistency, considers the well-known Mixture Theory to account for the presence of fibers in concrete microplanes. The model also accounts for bridging interactions of fibers in concrete cracks in the form of fiber-to-concrete bond-slip and dowel mechanisms. In this sense, the relevant role of the dowel mechanism in the bridging interaction of fiber in concrete when subjected to dominant shear was demonstrated in this work.

The numerical analyses demonstrate that the constitutive proposal captures the fundamental features of the mechanical behavior of SFRC. Very good agreements between numerical results against experimental data available in scientific literature have been achieved in terms of peak-strength and post-cracking toughness.

A distinguish feature of the proposed constitutive theory is its ability to evaluate non-homogeneous fiber distributions in the concrete matrix and moreover, their effect on both the post-peak load–displacement behavior and orientation evolution of the critical localization direction in the form of discontinuous bifurcation.

Acknowledgments

The authors acknowledge the financial support for this work by CONICET (National Council for science and technology) through the Grant PIP no. 112-2011010-1079 and by CIUNT (Research Council of the University of Tucuman, Argentina) through the Grant no. 26/E-511. The present study is also part of the activities carried out by the Authors within the "EnCoRe" Project (FP7-PEOPLE-2011-IRSES No. 295283; www.encore-fp7.unisa.it) funded by the European Union within the Seventh Framework Programme.

Appendix A. Analytical solution for localized failure in microplane-based elasto-plasticity

In the framework of the smeared crack approach, localized failure modes are related to discontinuous bifurcations of the equilibrium path, and lead to loss of ellipticity of the equations that govern the static equilibrium problem. The inhomogeneous or localized deformation field exhibits a plane of discontinuity that can be identified by means of the eigenvalue problem of the acoustic or localization tensor, see Ottosen and Runesson (1991). Analytical solutions for the discontinuous bifurcation condition, based on original works by Hadamard (1903), Thomas (1961) and Hill (1962), conduce to the macroscopic localization condition

$$det\,(\boldsymbol{Q}^{ep}) = 0 \tag{52}$$

being $\boldsymbol{Q}^{ep}$ the elasto-plastic localization tensor, define as

$$\boldsymbol{Q}^{ep} = \boldsymbol{N}\cdot\boldsymbol{E}^{ep}\cdot\boldsymbol{N}\,, \tag{53}$$

with $\boldsymbol{N}$, the normal direction to the discontinuity surface. According to Kuhl (2000), in case of microplane-based plasticity the macroscopic elasto-plastic tangent operator can be obtained analogously to the macroscopic stresses in Eq. (10), as

$$\boldsymbol{E}^{ep} = \frac{d\boldsymbol{\sigma}^{mac}}{d\boldsymbol{\varepsilon}^{mac}} = \frac{3}{4\pi}\int_{\Omega}\left[\boldsymbol{N}\otimes\frac{d\sigma_N}{d\varepsilon_N} + \boldsymbol{T}^T\cdot\frac{d\sigma_T}{d\boldsymbol{\varepsilon}_T}\right]d\Omega\,. \tag{54}$$

Regarding the microplane constitutive formulation in Section 2.3, the above equation can be expressed as

$$\boldsymbol{E}^{ep} = \boldsymbol{E}^{e} - \frac{3}{4\pi}\int_{\Omega}\frac{1}{h}\left[E_N\mu_N\boldsymbol{N} + E_T\,\boldsymbol{T}^T\cdot\boldsymbol{\mu}_T\right]\otimes\left[\nu_N E_N\boldsymbol{N} + E_T\,\boldsymbol{\nu}_T\cdot\boldsymbol{T}\right]d\Omega \tag{55}$$

being

$$h = E_N\,\nu_N\mu_N + E_T\boldsymbol{\nu}_T\cdot\boldsymbol{\mu}_T + H\,, \tag{56}$$

with the isotropic hardening/softening modulus H and

$$\nu_N = \frac{\partial\Phi}{\partial\sigma_N},\quad \mu_N = \frac{\partial\Phi^*}{\partial\sigma_N},\quad \boldsymbol{\nu}_T = \frac{\partial\Phi}{\partial\boldsymbol{\sigma}_T},\quad \boldsymbol{\mu}_T = \frac{\partial\Phi^*}{\partial\boldsymbol{\sigma}_T}. \tag{57}$$

The elastic macroscopic tangent operator is given by

$$\boldsymbol{E}^{e} = \frac{3}{4\pi}\int_{\Omega}E_N\boldsymbol{N}\otimes\boldsymbol{N} + E_T\,\boldsymbol{T}^T\cdot\boldsymbol{T}d\Omega\,. \tag{58}$$

Then, the elasto-plastic localization tensor in Eq. (53), results

$$\boldsymbol{Q}^{ep} = \boldsymbol{Q}^{e} - \frac{3}{4\pi}\int_{\Omega}\frac{\boldsymbol{a}^*\otimes\boldsymbol{a}}{h}d\Omega\,, \tag{59}$$

with the elastic localization tensor $\boldsymbol{Q}^e = \boldsymbol{N}\cdot\boldsymbol{E}^e\cdot\boldsymbol{N}$ and the traction vectors computed as

$$\begin{aligned}\boldsymbol{a} &= \left[\nu_N E_N\boldsymbol{N} + E_T\,\boldsymbol{\nu}_T\cdot\boldsymbol{T}\right]\cdot\boldsymbol{N},\\ \boldsymbol{a}^* &= \boldsymbol{N}\cdot\left[E_N\mu_N\boldsymbol{N} + E_T\,\boldsymbol{T}^T\cdot\boldsymbol{\mu}_T\right].\end{aligned} \tag{60}$$

Due to the complex structure of the acoustic tensor for microplane-based plasticity, the analytical assessment is not easy. Instead, numerical solutions must be applied and Eq. (59) can be rewritten as

$$\boldsymbol{Q}^{ep} \approx \boldsymbol{Q}^{e} - \sum_{l=1}^{n_{mp}}\left[\frac{\boldsymbol{a}^{*l}\otimes\boldsymbol{a}^{l}}{h^{l}}\right]\mathrm{w}^{l}. \tag{61}$$

References

Abrishambaf, A., Barros, J.A.O., Cunha, V.M.F.C., 2015. Tensile stress–crack width law for steel fibre reinforced self-compacting concrete obtained from indirect (splitting) tensile tests. Cem. Concr. Compos. 57, 153–165.
Bažant, Z.P., Di Luzio, G., 2004. Nonlocal microplane model with strain-softening yield limits. Int. J. Solids Struct. 41 (24–25), 7209–7240.
Bažant, Z.P., Gambarova, P.G., 1984. Crack shear in concrete: crack band microplane model. J. Struct. Eng. 110, 2015–2035.
Bažant, Z.P., Oh, B.H., 1983. Microplane model for fracture analysis of concrete structures. In: Proceedings of Symposium on the Interaction of Non-nuclearMunitions. U.S. Air Force Academy, Springs, pp. 49–55.
Bažant, Z.P., Oh, B.H., 1985. Microplane model for progressive fracture of concrete and rock. J. Eng. Mech. 111 (4), 559–582.
Beghini, A., Bažant, Z.P., Zhou, Y., Gouirand, O., Caner, F.C., 2007. Microplane model M5f for multiaxial behavior and fracture of fiber-reinforced concrete. J. Mater. Civil Eng. 133 (1), 66–75.
Brocca, M., Brinson, L.C., Bažant, Z.P., 2002. Three-dimensional constitutive model for shape memory alloys based on microplane model. J. Mech. Phys. Solids 50 (5), 1051–1077.
Caggiano, A., 2013. Meso-mechanical Analysis of Steel Fiber Reinforced Cementitious Composites, (Ph.D. thesis). Universita degli Studi di Salerno, Italy.
Caggiano, A., Etse, E., Martinelli, E., 2012. Zero-thickness interface model formulation for failure behavior of fiber-reinforced cementitious composites. Comput. Struct. 98-99, 23–32.
Caggiano, A., Martinelli, E., 2012. A unified formulation for simulating the bond behaviour of fibres in cementitious material. Mater. Des. 42, 204–213.
Caner, F.C., Bažant, Z.P., Wendner, R., 2013. Microplane model m7f for fiber reinforced concrete. Eng. Fract. Mech. 105, 41–57.
Carol, I., Bažant, Z.P., 1997. Damage and plasticity in microplane theory. Int. J. Solids Struct. 34 (29), 3807–3835.
Carol, I., Jirásek, M., Bažant, Z.P., 2001. A thermodynamically consistent approach to microplane theory. Part I. Free-energy and consistent microplane stresses. Int. J. Solids Struct. 38 (17), 2921–2931.
Carol, I., Jirasek, M., Bažant, Z.P., 2004. A framework for microplane models at large strain, with application to hyperelasticity. Int. J. Solids Struct. 41 (2), 511–557.
Carol, I., Prat, P., Bažant, Z.P., 1992. New explicit microplane model for concrete: theoretical aspects and numerical implementation. Int. J. Solids Struct. 29 (9), 1173–1191.
Cervenka, J., Bažant, Z.P., Wierer, M., 2005. Equivalent localization element for crack band approach to mesh-sensitivity in microplane model. Int. J. Numer. Methods Eng. 62 (5), 700–726.

Chern, J.C., Yang, H.J., Chen, H.W., 1992. Behavior of steel fiber-reinforced concrete in multiaxial loading. ACI Mater. J. 89 (1), 32–40.
Coleman, B.D., Gurtin, M.E., 1967. Thermodynamics with internal variables. J. Chem. Phys. 13, 597–613.
Coleman, B.D., Noll, W., 1963. The thermodynamics of elastic materials with heath conduction and viscosity. Arch. Rat. Mech. Anal. 13, 167–178.
Cunha, V., Barros, J., Sena-Cruz, J., 2012. A finite element model with discrete embedded elements for fibre reinforced composites. Comput. Struct. 94–95, 22–33.
Dei Poli, S., Di Prisco, M., Gambarova, P.G., 1992. Shear response, deformations, and subgrade stiffness of a dowel bar embedded in concrete. ACI Struct. J. 89 (6), 665–675.
Di Luzio, G., 2007. A symmetric over-nonlocal microplane model M4 for fracture in concrete. Int. J. Solids Struct. 44 (13), 4418–4441.
Dulacska, H., 1972. Dowel action of reinforcement crossing cracks in concrete. ACI Struct. J. 69 (12), 754–757.
El-Ariss, B., 2007. Behavior of beams with dowel action. Eng. Struct. 29 (6), 899–903.
Etse, G., Caggiano, A., Vrech, S., 2012. Multiscale failure analysis of fiber reinforced concrete based on a discrete crack model. Int. J. Fract. 178 (1–2), 131–146.
Etse, G., Nieto, M., 2004. Cosserat continua-based micro plane modelling. theory and numerical analysis. Latin Am. Appl. Res. 34, 229–240.
Etse, G., Nieto, M., Steinmann, P., 2003. A micropolar microplane theory. Int. J. Eng. Sci. 41 (13–14), 1631–1648.
Gal, E., Kryvoruk, R., 2011. Meso-scale analysis of FRC using a two-step homogenization approach. Comput. Struct. 89 (11–12), 921–929.
Gambarelli, S., Nisticò, N., Ožbolt, J., 2014. Numerical analysis of compressed concrete columns confined with CFRP: microplane-based approach. Compos. Part B: Eng. 67 (5), 303–312.
Gettu, R., 2008. Proceedings PRO60: International Symposium on Fiber Reinforced Concrete: Design and Applications – BEFIB 2008, Bagneux, France. RILEM Publications S.A.R.L.
Hadamard, J., 1903. Propagation des ondes et les equations d'Hydrodynamique. Chelsea, New York.
Hill, R., 1962. Acceleration waves in solids. J. Mech. Phys. Solids 1–16.
Hu, X.D., Day, R., Dux, P., 2003. Biaxial failure model for fiber reinforced concrete. J. Mater. Civil Eng. 15 (6), 609–615.
Kuhl, E., 2000. Numerische Modelle für Kohäsive Reibungsmaterialen, (Ph.D. thesis). Institut fur Baustatik der Universitat, Stuttgart.
Kuhl, E., Ramm, E., 2000. Microplane modelling of cohesive frictional materials. Eur J Mech. - A/Solids 19, 121–143.
Kuhl, E., Steinmann, P., Carol, I., 2001. A thermodynamically consistent approach to microplane theory. Part II. Dissipation and inelastic constitutive modeling. Int J of Solids and Structures 38 (17), 2933–2952.
Lee, S., Oh, J.H., Cho, J.Y., 2015. Compressive behavior of fiber-reinforced concrete with end-hooked steel fibers. Materials 8, 1442–1458.
Leite, J.P.B., Slowik, V., Mihashi, H., 2004. Computer simulation of fracture processes of concrete using mesolevel models of lattice structures. Cem. Concr. Res. 34 (6), 1025–1033.
Leukart, M., 2005. Kombinierte Anisotrope Schädigung und Plastizität bei kohäsiven Reibungsmaterialien, (Ph.D. thesis). Institut fur Baustatik der Universitat, Stuttgart.
Li, F., Li, Z., 2001. Continuum damage mechanics based modeling of fiber reinforced concrete in tension. Int. J. Solids Struct. 38 (5), 777–793.
Li, V.C., Lin, Z., Matsumoto, T., 1998. Influence of fiber bridging on structural size-effect. Int. J. Solids Struct. 35, 4223–4238.
Li, Z., Li, F., Chang, T.Y., Mai, Y.W., 1998. Uniaxial tensile behavior of concrete reinforced with randomly distributed short fibers. ACI Mater. J. 564–574.
Mirsayah, A., Banthia, N., 2002. Shear strength of steel fiber-reinforced concrete. ACI Mater. J. 5, 473–479.
Naaman, A., Reinhardt, H., 2006. Proposed classification of HPFRC composites based on their tensile response. Mater. Struct. 39, 547–555.
Nataraja, M.C., Dhang, N., Gupta, A.P., 1999. Stress–strain curves for steel–fiber reinforced concrete under compression. Cem. Concr. Compos. 21, 383–390.
Neves, R.D., de Almeida J. C. O., F., 2005. Compressive behaviour of steel fibre reinforced concrete. Struct. Concr. 6, 1–8.
Nguyen, A.D., Stoffel, M., Weichert, D., 2010. A one-dimensional dynamic analysis of strain-gradient viscoplasticity. Eur. J. Mech. - A/Solids 29 (6), 1042–1050.
Oliver, J., Linero D. L. ans Huespe, A.E., Manzoli, O.L., 2008. Two-dimensional modeling of material failure in reinforced concrete by means of a continuum strong discontinuity approach. Comput. Methods Appl. Mech. Eng. 197, 332–348.
Oliver, J., Mora, D.F., Huespe, A.E., Weyler, A., 2012. A micromorphic model for steel fiber reinforced concrete. Int. J. Solids Struct. 197, 2990–3007.
Ottosen, S., Runesson, K., 1991. Properties of discontinuous bifurcation solutions in elasto-plasticity. Int. J. Solids Struct. 27, 401–421.
Ožbolt, J., Li, Y., Kozar, I., 2001. Microplane model for concrete with relaxed kinematic constraint. Int. J. Solids Struct. 38 (16), 2683–2711.
Park, H., Kim, H., 2003. Microplane model for reinforced-concrete planar members in tension-compression. J. Struct. Eng. 337–345.
Prasad, M.V.K., Krishnamoorthy, C., 2002. Computational model for discrete crack growth in plain and reinforced concrete. Comput. Methods Appl. Mech. Eng. 191 (25–26), 2699–2725.
di Prisco, M., Plizzari, G., Vandewalle, L., 2009. Fiber reinforced concrete: new design perspectives. Mater. Struct. 42, 1261–1281.
Radtke, F.K.F., Simone, A., Sluys, L.J., 2010. A computational model for failure analysis of fiber reinforced concrete with discrete treatment of fibers. Eng. Fract. Mech. 77 (4), 597–620.
Schauffert, E.A., Cusatis, G., 2012. Lattice discrete particle model for fiber reinforced concrete (LDPM-F). I: theory. J. Eng. Mech. 138 (7), 826–833.
Seow, P.E.C., Swaddiwudhipong, S., 2005. Failure surface for concrete under multiaxial load – a unified approach. J. Mater. Civil Eng. 17 (2), 219–228.
Soltanzadeh, F., Barros, J.A.O., Santos, R.F.C., 2015. High performance fiber reinforced concrete for the shear reinforcement: experimental and numerical research. Constr. Build. Mater. 77, 94–109.
Soroushian, P., Obaseki, K., Rojas, M.C., 1987. Bearing strength and stiffness of concrete under reinforcing bars. ACI Mater. J. 84 (3), 179–184.
Thomas, T., 1961. Plastic Flow and Fracture in Solids. Academic Press, London.
Truesdell, C., Toupin, R., 1960. The classical field theories, III/I. Handbuch der Physik. Springer-Verlag, Berlin.
Vrech, S., Etse, G., 2009. Gradient and fracture energy-based plasticity theory for quasi-brittle materials like concrete. Comput. Methods Appl. Mech. 199 (1–4), 136–147.
Vrech, S., Etse, G., Meschke, G., Caggiano, A., Martinelli, E., 2010. Meso- and macroscopic models for fiber-reinforced concrete. In: Computational Modelling of Concrete Structures, Rohrmoos/Schladming, Austria, pp. 241–250.